Incorporation of MRI-AIF Information For Improved Kinetic Modelling of Dynamic PET Data

Hasan Sari, *Student Member, IEEE*, Kjell Erlandsson, Kris Thielemans, *Senior Member, IEEE*, David Atkinson, Sebastien Ourselin, Simon Arridge, and Brian F. Hutton, *Senior Member, IEEE*

***Abstract*—In the analysis of dynamic PET data, compartmental kinetic analysis methods require an accurate knowledge of the arterial input function (AIF). Although arterial blood sampling is the gold standard of the methods used to measure the AIF, it is usually not preferred as it is an invasive method. An alternative method is the simultaneous estimation method (SIME), where physiological parameters and the AIF are estimated together, using information from different anatomical regions. Due to the large number of parameters to estimate in its optimisation, SIME is a computationally complex method and may sometimes fail to give accurate estimates. In this work, we try to improve SIME by utilising an input function derived from a simultaneously obtained DSC-MRI scan. With the assumption that the true value of one of the six parameter PET-AIF model can be derived from an MRI-AIF, the method is tested using simulated data. The results indicate that SIME can yield more robust results when the MRI information is included with a significant reduction in absolute bias of K_i estimates.**

***Index Terms*—Arterial input function, magnetic resonance imaging, noninvasive measurement, positron emission tomography.**

I. Introduction

In THE pharmacokinetic analysis of dynamic positron emission tomography (PET) images, compartmental models are widely used to quantify physiological and biochemical processes in the tissue of interest. This requires an accurate estimation of the tracer concentration in plasma as a function of time, which is known as the arterial input function (AIF).

There are several existing methods used to measure the input function. The gold standard method involves collection of arterial blood samples at various time points, which are further analyzed in the laboratory environment to measure the total concentration of non-metabolized tracer in plasma [1]. However, this method is not favoured in routine clinical practice, as it is highly invasive and labour intensive. For this reason, a number of alternative methods have been proposed to accurately measure the input function. One method is the use of standardized, population-based input functions from literature, which is obtained by taking the average of the AIF curves from a group of patients [2]. The method can be improved by taking one or more arterial blood samples to scale the population-based input function [3], [4]. However, this method assumes that input functions can be approximated using a standard input function, which may not always be valid. Input functions of different individuals, or different groups, will always have some shape discrepancies, which may cause errors in parameter estimation. In addition, to our knowledge, this method has only been applied to 2-deoxy-2-[^{18}F] fluoro-D-glucose (FDG) studies, so has limited usage with other tracers. A third method is to obtain image-derived input functions (IDIF) [5] where the voxels corresponding to arteries, or heart, are defined on PET images, and the mean concentration within that region is computed over time. This method completely avoids the need for collecting blood samples but introduces the difficulties of correctly segmenting the arteries on PET images with low spatial resolution and correcting for partial volume effects. There has been some work to improve this method by using higher resolution co-registered MRI images in the segmentation of arteries and correction for partial volume effects [6], [7]. In addition, a visible artery may not always be present in the field of view. Finally, this method is less useful if radiometabolites are present in the plasma, as they will contribute to the signal in the PET images and the IDIF method can not distinguish the fraction of the parent compound from the total blood activity.

Another alternative to measure the input function is the simultaneous estimation (SIME) method [8], [9], [10], where multiple region of interests (ROIs) are utilized. Assuming that the input function is common between these regions, input function parameters are estimated simultaneously with the kinetic parameters for all ROIs. In this approach, the objective function includes the input function parameters as well as kinetic parameters, and takes strength from the distinct kinetic behaviour of each region. In order to ensure model identifiability, this method requires at least one blood sample (a venous sample may be sufficient) which is used to scale the estimated input function. The biggest disadvantage of the SIME method in the PET kinetic analysis is its computational complexity as there are a large number of parameters to estimate in the optimization (input function parameters plus kinetic parameters for each region).

An accurate measurement of the input function is also essential in the analysis of dynamic-susceptibility contrast (DSC)

Manuscript received September 30, 2014; revised February 10, 2015; accepted April 04, 2015. Date of publication June 02, 2015; date of current version June 12, 2015.

H. Sari, K. Erlandsson, and K. Thielemans are with the Institute of Nuclear Medicine, University College London, London NW1 2BU, U.K. (e-mail: hasan.sari.12@ucl.ac.uk).

D. Atkinson is with the Centre for Medical Imaging, University College London, London NW1 2PG, U.K.

S. Ourselin and S. Arridge are with the Centre for Medical Image Computing, University College London, London WC1E 6BT, U.K.

B. F. Hutton is with the Institute of Nuclear Medicine, University College London, London NW1 2BU, U.K., and also with the Centre for Medical Radiation Physics, University of Wollongong, Wollongong NSW 2522, Australia.

Digital Object Identifier 10.1109/TNS.2015.2426952

MRI and dynamic contrast enhanced (DCE) MRI. In these techniques, the injected bolus of gadolinium-based contrast agent causes a signal drop on T2 and T2* weighted images and a signal rise on T1 weighted images. These signal changes can then be related to the time-dependent concentration of the contrast agent [11]. Estimation of the input function can have some advantages in MRI due to its temporal resolution. In DSC-MRI, the temporal resolution can be set to 1 second [12] which makes it easier to detect the rapid changes during the first passage of the contrast agent. On the other hand, the nonlinear relationship between the measured MRI signal and contrast agent concentration can be a problem in MRI quantification, as opposed to PET where a linear relationship exists.

In this work, we tried to reduce the complexity of the PET SIME method by deriving some of the input function parameters from an input function measured from a simultaneous dynamic MRI scan. If the same injection protocols are used, the early parts of PET derived and MRI derived input functions will have similar shapes, since the delivery of tracer or contrast agent to the tissue of interest will be mainly dominated by vascular flow dynamics [13], [14].

II. Theory

A. Compartment Model

In this work, a dynamic FDG model was adopted to simultaneously extract kinetic parameters together with the input function. The behaviour of FDG after injection can be described using a two-tissue compartment model [15] as illustrated in Fig. 1. In this model, one compartment represents the extravascular space of the tissue, which contains the free tracer available for metabolism, and a second compartment represents the concentration of the metabolised tracer. This model was used in our simulation study.

The two-tissue compartment model can be described using ordinary differential equations, which are:

$$\frac{\mathrm{d}C_{\mathrm{F}}(t)}{\mathrm{d}t} = K_1 C_{\mathrm{P}}(t) + k_4 C_{\mathrm{M}}(t) - (k_2 + k_3) C_{\mathrm{F}}(t) \quad (1)$$

$$\frac{\mathrm{d}C_{\mathrm{M}}(t)}{\mathrm{d}t} = k_3 C_{\mathrm{F}}(t) - k_4 C_{\mathrm{M}}(t) \quad (2)$$

where K_1, k_2, k_3 and k_4 are the rate constants, C_p is the concentration of tracer in the plasma, or the input function, C_F is the concentration of the free tracer and C_M is the concentration of the phosphorylated FDG in the tissue of interest. In the absence of vascular tissue in the region of interest, the sum of C_F and C_M gives us the total tissue activity, C_i. The solution of the $C_i(\mathrm{t})$ is given by:

$$C_{\mathrm{i}}(t) = \left(\phi_1 e^{-\theta_1 t} + \phi_2 e^{-\theta_2 t}\right) \otimes C_{\mathrm{P}}(t) \quad (3)$$

where

$$\theta_{1,2} = \frac{1}{2}\left(k_2 + k_3 + k_4 \mp \sqrt{(k_2 + k_3 + k_4)^2 - 4k_2 k_4}\right)$$

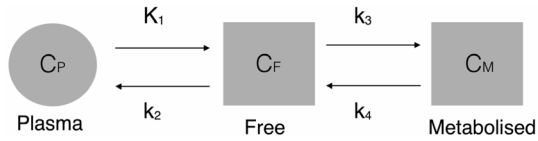

Fig. 1. Schematic diagram of the reversible two-tissue compartment model used for FDG data.

and

$$\phi_1 = K_1 \frac{k_3 + k_4 + \theta_1}{\theta_2 - \theta_1}$$

$$\phi_2 = -K_1 \frac{k_3 + k_4 + \theta_2}{\theta_2 - \theta_1}$$

$\theta_{1,2}$ and $\phi_{1,2}$ are the parameters of the solution which are the combinations of rate constants. Once $\mathrm{C}_i(\mathrm{t})$ and $\mathrm{C}_P(\mathrm{t})$ are known for several time points, it is possible to estimate the rate constant values by non-linear least squares fitting.

In addition to the activity in the tissue, total activity measured by the PET scanner also includes the activity from the vascular tissue present in the region of interest. This vascular activity, or blood volume, can sometimes be high enough to cause errors in the estimated kinetic parameters and needs to be taken into account in the model [16]. Therefore, the total observed activity, $C_T(\mathrm{t})$ can be written as:

$$C_{\mathrm{T}}(t) = ((1 - \mathrm{BV}) \cdot C_{\mathrm{i}}(t) + \mathrm{BV} \cdot C_{\mathrm{wb}}(t)) e^{-\lambda t} \quad (4)$$

where λ is the radioactive decay constant for the radionuclide, BV represents the blood volume and C_{wb} represents the concentration of tracer in whole blood. BV can sometimes be a parameter of interest and can be estimated together with rate constants.

$$K_{\mathrm{i}} = \frac{K_1 k_3}{k_2 + k_3} \quad (5)$$

Once the values of rate constants ($K_1 - k_4$) are estimated, the net influx constant, K_i, can be calculated using equation (5). Influx rate is a representation of rate constants in a non-directional way, and incorporates both net inward transport and trapping of the tracer in tissue of interest.

B. Input Function

Arterial input functions are usually measured by taking a number of blood samples at different time points, in order to determine the concentration of the PET tracer or MRI contrast agent in the blood plasma over time. A good estimation of AIF is essential for accuracy of results in both PET and MRI kinetic analyses.

AIFs can also be represented by mathematical models which are used to fit blood data. One example is Feng's mathematical model which is a sum of a gamma variate with biexponential [2]. It has six parameters and can be written as equation (6)

$$C_{\mathrm{P}}(t) = (A_1 t - A_2 - A_3) e^{-\lambda_1 t} + A_2 e^{-\lambda_2 t} + A_3 e^{-\lambda_3 t} \quad (6)$$

where λ_1, λ_2 and λ_3 are the eigenvalues of the model and A_1, A_2 and A_3 are the coefficients of the model.

With the introduction of hybrid PET/MRI scanners, dynamic PET and MRI data can be obtained simultaneously. Hence, it is possible to measure the PET-AIF and MRI-AIF during the same scan. At the moment, PET tracers and MRI contrast agent injections are administered separately, and to our knowledge no group has tried delivering both with a single injection in a clinical scan. However if the PET tracer and the MRI contrast agent are injected using the same injection protocol (i.e. same injection duration), similar peak shapes are expected to be seen in PET and MRI input functions, after scaling them to same peak heights. Ibaraki *et al.* [13] have shown this with input functions from $H_2^{15}O$ PET and DSC-MRI studies. Poulin *et al.* [14] have also observed this similarity on input functions obtained from mice studies and they have also shown that an AIF conversion from PET-AIF to MRI-AIF or vice versa is possible in specific circumstances.

If the obtained PET and MRI input functions are fitted using equation (6), then similar values are expected for the λ_1 parameter due to the similarity in the bolus shapes. Hence, it can be assumed that even in the absence of a PET-AIF, the λ_1 parameter can be determined if an MRI-AIF is present from the same study. This information can be used in SIME to reduce the number of AIF parameters to estimate by one.

III. Materials and Methods

A. Generation of Simulation Data

The purpose of this work was to improve the results of the simultaneous estimation work, by reducing some of the parameters in the optimization using information from an MRI derived input function. Methods with and without the MRI information were compared using simulation.

Simulated data were created by using COMKAT, version 3.2[17] in MATLAB (The Mathworks, Inc., Natick, MA), version 8.1.0. Feng's function was used as the plasma input [2] with published averaged parameter values: $A_1 = 851.1225$, $A_2 = 21.8798$, $A_3 = 20.8113$, $\lambda_1 = 4.1339$, $\lambda_2 = 0.1191$ and $\lambda_3 = 0.0104$. No time delay was assumed in the delivery of the input function. Time activity curves (TACs) were generated using a two-tissue compartment model equation, using kinetic parameters and cerebral blood volume values from a published human brain FDG study, as shown in Table I [16]. Rate constant values from grey matter, white matter and tumour regions were used and the resulting TACs are illustrated as data A, data B and data C respectively in Fig. 2. The simulated AIF and TACs were sampled at 29 time intervals. The acquisition protocol was set to 6 frames of 5 sec, 2×15 sec, 6×30 sec, 3×2min, 2×5min and 10×10min, summing to a total scanning duration of 2 hours.

Gaussian noise with standard deviation, σ, was generated based on PET measurement variance structure as shown in equation (7) [18].

$$\sigma(t) = \sqrt{\frac{\alpha^2 . C_{\mathrm{T}}(t)}{\Delta t_k}} \tag{7}$$

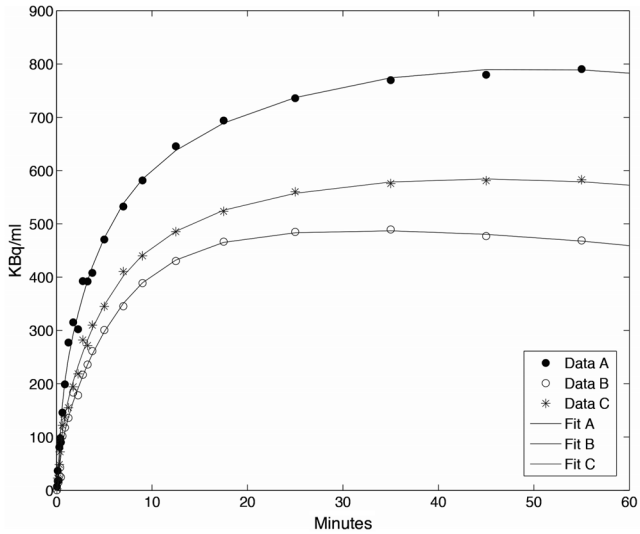

Fig. 2. Simulated time activity curves with an example of their fits. Noise level was set to 0.5. Data A represents the time activity curve generated using kinetic parameters from the grey matter, data B from the white matter and Data C from the tumour region. Only the first hour is plotted for simplicity.

TABLE I
True Values of the Kinetic Parameters used to Generate the Three Time Activity Curves

	Grey Matter	White Matter	Tumour
K_1 (mL.cm^{-3}.min^{-1})	0.041	0.023	0.028
k_2 (min^{-1})	0.120	0.073	0.087
k_3 (min^{-1})	0.064	0.034	0.047
k_4 (min^{-1})	0.0075	0.0098	0.0084
K_i (mL.cm^{-3}.min^{-1})	0.0143	0.0073	0.0098
BV (ml/100g)	5.80	2.50	4.40

where C_T is the total measured PET activity, Δt_k is the frame duration and α is the scaling factor used to set the noise level added to the data. In this work, three noise levels were considered and α was set to 0.5, 2 and 4 respectively. The lowest noise level corresponds to a smooth time activity curve with a low amount of noise, which is typical when very large ROIs are used. The highest noise level corresponds to typical noisy data when TACs are extracted from a few voxels. Fifty realizations were created for each noise level.

B. Optimization of the Cost Function

The SIME cost function includes common input function parameters between all regions, together with kinetic parameters from different ROIs, which are estimated simultaneously. The cost function can be written as equation (8):

$$\phi(p) = \sum_{i=1}^{n} \sum_{j=1}^{m} \left[E_i(t_j) - M_i(t_j)\right]^2 \tag{8}$$

where n is the number of regions, m is the number of time points in each TAC, E is the measured concentration of the

tracer in the region at time point t_j and M is the model output with parameter vector p, which includes 5 parameters (K_1, k_2, k_3, k_4 and BV) from each region of interest and 6 parameters ($A_1, A_2, A_3, \lambda_1, \lambda_2, \lambda_3$) from the AIF model.

The objective function was optimized using the ordinary least squares method (OLS), where the best estimates of parameters are found by minimizing the cost function. Weights determined from variance structure (eq. (7)) were not used in the optimization as uniform weighting of OLS gave results with lower bias on estimated paraeters [19]. Optimization was performed by using *fmincon* from the MATLAB Optimization Toolbox via COMKAT's interface.

C. Scaling of the Input Function

In the simultaneous estimation method, one or more arterial or venous blood samples are required to scale the input function. In the implementation of their method, Feng *et al.* used multiple blood samples to aid the recovery of AIF. As A_3 and λ_3 dominate the tail of the AIF model, which represents the end of the scanning period, it can be assumed that these parameters can be obtained by fitting two or more blood samples measured near the end of scanning. In this simulation work, parameters A3 and λ_3 were kept fixed to their true values in order to reproduce the effect of this scaling method on the parameter estimates.

An alternative AIF scaling method was also implemented, where only one blood sample is obtained at the end of the scan. Then, the ratio of estimated AIF's endpoint to the actual radioactive tracer concentration obtained by blood sample is used as a factor to scale the whole input function. This was simulated by computing the ratio of true input function endpoint to estimated input function endpoint and multiplying the whole input function with this ratio.

D. Analysis of Parameter Estimates

The simulation study was repeated 5 times using the simulated dataset at each of 3 noise levels. The five different experimental scenarios can be listed as following:

1) No MRI information, single point AIF normalization
2) With MRI information, single point AIF normalization
3) No MRI information, multiple point AIF normalization
4) With MRI information, multiple point AIF normalization
5) Input function parameters fixed to their true values

AIF parameters and rate constants, together with the blood background, were estimated for each of 50 noise realizations. In the fifth case, all of the six AIF parameters were fixed to their true values and only the kinetic parameters were estimated. This was done in order to see the accuracy of estimated parameters when the perfect AIF was used.

For each case, absolute bias and coefficient of variation (CV) values were calculated and used in the performance comparison. These were calculated by using equations (9) and (10) respectively, where, $\overline{P}$ represents the mean parameter over 50 noise realizations, $SD_{\overline{P}}$ represents the standard deviation of $\overline{P}$ and P^{true} is the true value of the parameter.

$$\mathrm{CV}_{\overline{P}} = \frac{SD_{|P|}}{|\overline{P}|} \times 100\% \tag{9}$$

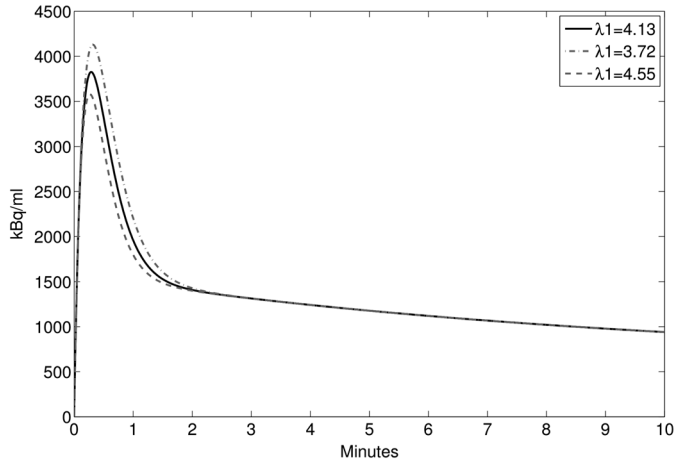

Fig. 3. Simulated arterial input function with different λ_1 values. λ_1 was set to 4.134 to represent Feng's AIF model. AIFs with $\pm 10\%$ error on λ_1 are also shown to model the effect of error in the AIF.

$$\mathrm{Bias} = \left| \frac{P^{\mathrm{true}} - \overline{P}}{P^{\mathrm{true}}} \right| \times 100\% \tag{10}$$

E. Sensitivity Analysis

Even though bolus shapes of PET-AIF and MRI-AIF are expected to be similar, there might be small differences in the derived parameters when both input functions are fitted with the model. This can cause PET λ_1 values to be underestimated or overestimated from the MRI-AIF. The effect of any error present in the fixed λ_1 parameter on the parameter estimates was evaluated.

By adding $\pm 10\%$ error on the fixed λ_1 parameter, λ_1 was set to 3.7206 and 4.5474 respectively. All the starting parameters, lower and upper bounds, and optimization settings were kept the same as in the previous experiment. Fig. 3 illustrates how the AIF changes with different λ_1 values.

F. Inter-individual Variability Analysis

In order to further evaluate the performance of the method, the simulation study was repeated with four other sets of rate constants obtained from various published FDG brain tumour studies (group 2 from [20] group 3 and 4 from [21], and group 5 from [22]). Similar to the first study, rate constants were obtained from grey matter, white matter and tumour tissue (Range of K_1: 0.023-0.10, k_2: 0.087-0.162, k_3: 0.032-0.107, k_4: 0.001-0.15, BV: 0.3-0.7). TACs were generated using these rate constants and Feng's input function and gaussian noise was added to the generated TACs.

IV. Results

A. Evaluation of Parameter Estimates

The average bias on kinetic parameters of each ROI is shown in Fig. 4 for each of the 5 methods and noise levels used. It can be seen that when no AIF parameter was fixed and AIF scaling with a single blood sample was used, the average bias on the K_i estimates, averaged over three noise levels, was approximately 13.8%. This was reduced to 5.4% when the λ_1 parameter of AIF

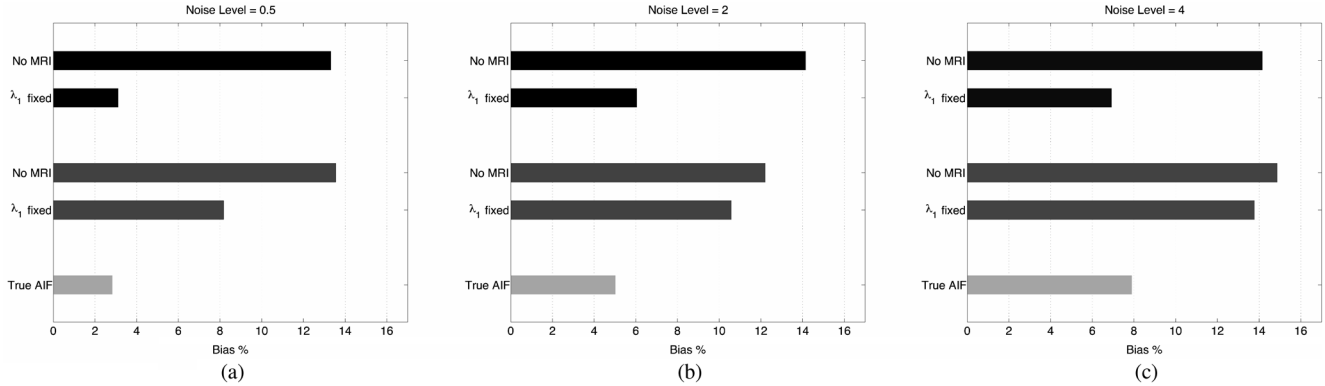

Fig. 4. Absolute bias on 50 K_i estimates, averaged over three ROIs, when noise level was set to (a) 0.5, (b) 2, (c) 4. Black bars on top show the bias with the scaling method with one blood sample obtained at the end of the study, dark grey bars show the bias with the scaling method where the tail is fit to the multiple blood samples obtained towards the end of the study and light grey bars show the bias which would be present when all six parameters of the AIF was set to their true values.

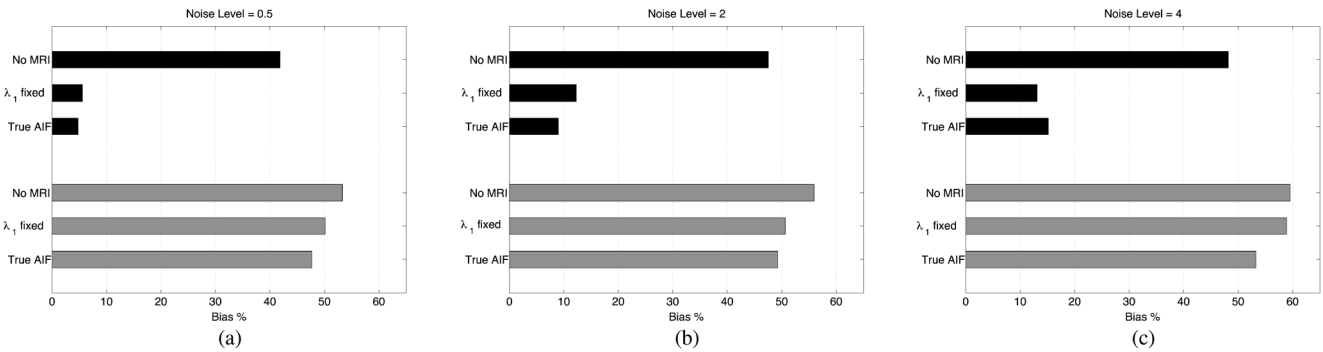

Fig. 5. Absolute bias on 50 K_1 and an average of the k_2, k_3 and k_4 parameter estimates, averaged over three ROIs. Results are shown for noise levels (a) 0.5, (b) 2, (c) 4. Only one blood sample AIF normalisation results are shown. Black bars indicate the bias on K_1 estimates and grey bars indicate the average bias on $k_2 - k_4$ estimates.

was fixed to its true value. When the AIF was scaled using the method where the tail was fit to multiple blood samples, the average bias was 13.5% and was reduced to 10.6% after λ_1 was fixed to its true value. The average bias on the estimated K_i was 5.2% when all six parameters of the input function were set to their true values and only values of the kinetic parameters and the vascular fraction for each ROI were estimated. The same trend was seen at all noise levels. Also the biases of the fits were close to the bias with true input function when one input function parameter was obtained from MRI-AIF. However the observed improvement was decreased as the noise level increased.

When the biases of individual rate constant estimates were studied, it was seen that fixing the λ_1 parameter improved the K_1 estimates most. When the single blood sample AIF scaling method was used, the bias on K_1 was reduced from 46.3% to 10.3%, averaged over all noise levels. When the alternative AIF scaling method was used, 58.6% bias was seen on K_1 estimates even after the λ_1 parameter was fixed to its true value. The bias of parameters k_2, k_3, k_4 and BV were comparable across the two AIF scaling methods. For these parameters, much smaller improvement was observed after the MRI component was utilized. These are also shown in Fig. 5. BV estimates had 66.8% absolute bias which was reduced to 64.8% when λ_1 parameter was fixed to its true value for the single point AIF normalisation method. However, the high bias on the BV did not affect the accuracy of K_i estimates. This was confirmed by a seperate experiment by estimating the K_i with BV fixed to its true value where only 0.28% increase in overall bias was observed.

Fig. 6 shows the summary of coefficient of variation of estimated K_i parameters, averaged over three ROIs and plotted for each noise level. From these results, it can be seen that both AIF scaling methods yielded K_i estimates with similar CV values. Using the scaling method with a single blood sample resulted in K_i estimates with 6.3% CV, averaged over three noise levels, which was reduced to 5.7% with fixed λ_1. The AIF scaling method with multiple blood samples produced K_i estimates with 6.7% CV and this was improved to 5.4%. Finally, the true input function estimated the influx rate parameter with average CV of 4%.

B. Sensitivity Analysis Results

In this section, the effect of erroneous AIF on the kinetic parameter estimates is evaluated. Similar to previous analyses, absolute bias and coefficient of variation are used to compare estimates.

Fig. 7 shows the bias when the λ_1 was underestimated or overestimated by 10%. Results obtained with the single blood sample AIF scaling method are shown only. Bias on parameter estimates obtained with no λ_1 fixing and when λ_1 was fixed to

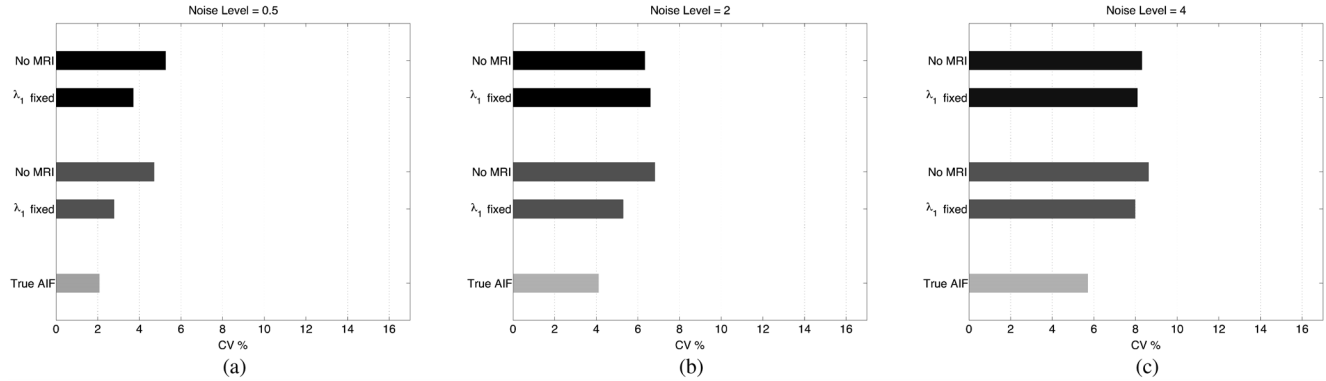

Fig. 6. Coefficient of variation values over 50 K_i estimates, averaged over three ROIs, when noise level was set to (a) 0.5, (b) 2, (c) 4. Black bars on top show the CV with the scaling method with one blood sample obtained at the end of the study, dark grey bars show the CV with the scaling method where the tail is fit to the multiple blood samples obtained towards the end of the study and light grey bars show the CV which would be present when all six parameters of the AIF was set to their true values.

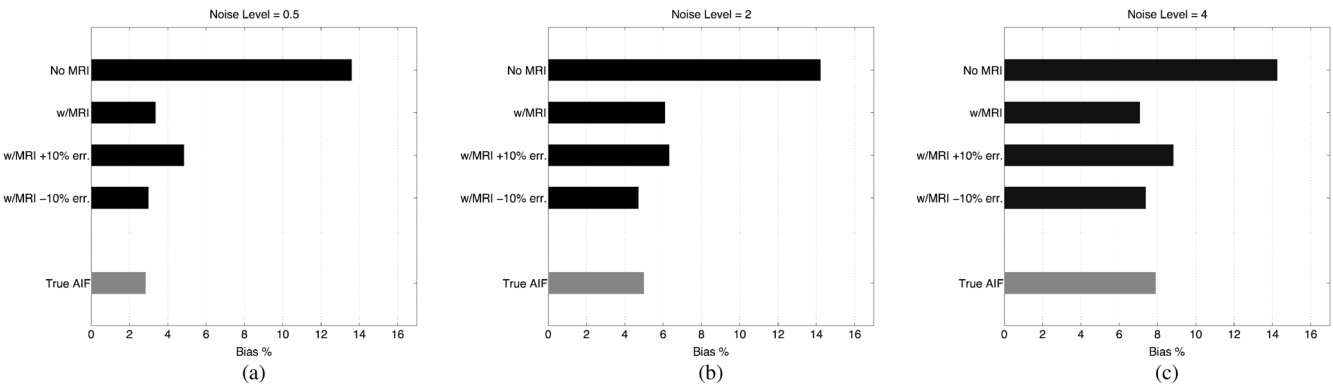

Fig. 7. Absolute bias on estimated Ki values. Darker bars show results without the MRI component, one PET-AIF parameter fixed assuming it can be obtained from MRI-AIF, $\pm 10\%$ error added on the fixed AIF parameter. Grey bars show the bias on estimates when all the AIF parameters were fixed to their true values.

its true value are also included in the plot for comparison purposes. These results showed that much lower bias values were obtained even when $\pm 10\%$ error was present in the fixed AIF parameter. The method estimated rate constants more accurately when the λ_1 was underestimated rather than overestimated.

C. Inter-individiual Variability Analysis

Fig. 8 shows the absolute bias on K_i estimates obtained in 5 different simulation studies with TACs generated with different sets of rate constants. Results with the single blood sample AIF normalisation method is included only. Significant reduction in absolute bias of estimates was obtained by fixing λ_1 to its true value in all of the 5 different simulation studies. It can be seen that including the MRI information reduced the bias in the range of 3.4% to 12%.

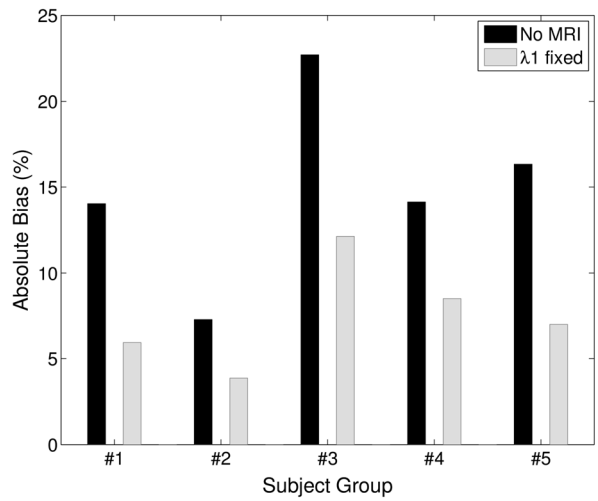

Fig. 8. Results of the inter-individual variability analysis. Reduction in absolute bias of K_i estimates after fixing λ_1 to its true value are shown for five different simulation studies. Results for noise level 2 and single point AIF normalisation method are shown only. Black bars show the results with no MRI information and grey bars denotes the results with λ_1 fixed.

V. Discussion and Conclusions

We have proposed a novel approach for improving AIF estimation, and hence kinetic parameter estimation in dynamic FDG-PET studies with the SIME method by utilising information from simultaneously acquired DSC-MRI data. We used simulated data to compare estimated parameters with and without additional MRI information. With the single-point AIF normalisation method, the bias in the K_i values was reduced by 77%, 57% and 51% respectively for each noise level using the proposed method, to a level similar to that obtained with fully know AIFs. For single blood sample AIF normalisation method, utilising the MRI information gave slightly better results than true AIF results at the highest noise level. A similar

behaviour was also seen for the K_1 estimates. A paired t-test comparison of the absolute error in individual K_1 estimates obtained with both methods showed that the difference in both sets of estimates is not statistically significant, with p values of 0.09, 0.37 and 0.23 for the three ROIs.

The improvement in K_i biases was insensitive to small errors in the fixed values of $\lambda_1(\pm 10\%)$. The bias-reduction was much lower when the more complex normalisation procedure was used, which involves collecting multiple blood samples in practice. The biggest improvement was seen in the K_1 estimates. The variance in K_i was reduced only in the low-noise case. The reduction was slightly larger with the more complex normalisation.

In this work, the assumption of similarity between PET-AIF and MRI-AIF peaks was based on the similar rates of delivery of PET tracer and MRI contrast agent to the tissue of interest as this is mostly dominated by cardiac output and blood flow. This would be valid for most of the PET tracers with negligible uptake in lungs. The AIF peak shapes also depend on the injection durations used; the administration of tracer and contrast agent are usually performed separately with different injection rates. The effect of different injection durations on PET-AIF and MRI-AIF peak shapes needs to be taken into account before a parameter conversion can be made. We have shown that parameters describing the early part of the PET-AIF can be derived from an MRI-AIF even when different injection durations are used [23].

In addition to FDG studies, the SIME method is a promising approach to analyse other tracers [9][10]. As the metabolite-free AIF can be measured using this method, it can potentially be used to study tracers with radio-labelled metabolites present in the blood.

In conclusion, we have shown that the accuracy of kinetic parameter estimation by the SIME method can be improved using data from a DSC-MRI derived AIF. The method requires a single blood-sample at the end of the scan for AIF normalisation.

REFERENCES

[1] L. Sokoloff, M. Reivich, C. Kennedy, M. H. Des Rosiers, C. S. Patlak, K. D. Pettigrew, O. Sakurada, and M. Shinohara, "The [14C]deoxyglucose method for the measurement of local cerebral glucose utilization: Theory, procedure, and normal values in the conscious and anesthetized albino rat," *J. Neurochem.*, vol. 28, pp. 897–916, 1977.

[2] D. Feng, X. Wang, and H. Yan, "A computer simulation study on the input function sampling schedules in tracer kinetic modeling with positron emission tomography (PET)," *Comput. Methods Programs Biomed.*, vol. 45, no. 3, pp. 175–186, Nov. 1994.

[3] S. Takikawa, V. Dhawan, P. Spetsieris, W. Robeson, T. Chaly, R. Dahl, D. Margouleff, and D. Eidelberg, "Noninvasive quantitative fluorodeoxyglucose PET studies with an estimated input function derived from a population-based arterial blood curve," *Radiology*, vol. 188, pp. 131–136, 1993.

[4] S. Eberl, A. R. Anayat, R. R. Fulton, P. K. Hooper, and M. J. Fulham, "Evaluation of two population-based input functions for quantitative neurological FDG PET studies," *Eur. J. Nucl. Med.*, vol. 24, pp. 299–304, 1997.

[5] P. Zanotti-Fregonara, K. Chen, J.-S. Liow, M. Fujita, and R. B. Innis, "Image-derived input function for brain PET studies: Many challenges and few opportunities," *J. Cerebral Blood Flow Metabol.*, vol. 31, pp. 1986–1998, 2011.

[6] N. da Silva, H. Herzog, C. Weirich, L. Tellmann, E. R. Kops, H. Hautzel, and P. Almeida, "Image-derived input function obtained in a 3tmr-brainpet," *Nucl. Instrum. Methods Phys. Res. A*, vol. 702, pp. 22–25, 2013.

[7] E. K. Fung and R. E. Carson, "Cerebral blood flow with [15O]water PET studies using an image-derived input function and MR-defined carotid centerlines," *Phys. Med. Biol.*, vol. 58, no. 6, pp. 1903–1923, Mar. 2013.

[8] D. Feng, K. P. Wong, C. M. Wu, and W. C. Siu, "A technique for extracting physiological parameters and the required input function simultaneously from PET image measurements: Theory and simulation study," *IEEE Trans. Inf. Technol. Biomed.*, vol. 1, no. 4, pp. 243–254, Dec. 1997.

[9] K. P. Wong, D. Feng, S. R. Meikle, and M. J. Fulham, "Simultaneous estimation of physiological parameters and the input function–in vivo PET data," *IEEE Trans. Inf. Technol. Biomed.*, vol. 5, no. 1, pp. 67–76, Mar. 2001.

[10] R. T. Ogden, F. Zanderigo, S. Choy, J. J. Mann, and R. V. Parsey, "Simultaneous estimation of input functions: An empirical study," *J. Cerebral Blood Flow Metabol.*, vol. 30, no. 4, pp. 816–826, Apr. 2010.

[11] M. Essig, T. B. Nguyen, M. S. Shiroishi, M. Saake, J. M. Provenzale, D. S. Enterline, N. Anzalone, A. Dörfler, A. Rovira, M. Wintermark, and M. Law, "Perfusion MRI: The five most frequently asked clinical questions," *Amer. J. Roentgenol.*, vol. 201, pp. 495–510, 2013.

[12] F. Calamante, "Arterial input function in perfusion mri: A comprehensive review," *Prog. Nucl. Magn. Reson. Spectrosc.*, vol. 74, pp. 1–32, 2013.

[13] I. K. M. Ibaraki, E. Shimosegawa, H. Toyoshima, K. Ishigame, S. Sugawara, K. Takahashi, and S. Miura, "Evaluation of arterial input function for Perfusion MRI: Comparison with that of PET study," in *Proc. Int. Soc. Mag. Reson*, 2005, vol. 13, no. 1, p. 1125.

[14] E. Poulin, R. Lebel, E. Croteau, M. Blanchette, L. Tremblay, R. Lecomte, M. Bentourkia, and M. Lepage, "Conversion of arterial input functions for dual pharmacokinetic modeling using Gd-DTPA/MRI and 18F-FDG/PET," *Magnet. Resonance Med.*, vol. 69, pp. 781–792, 2013.

[15] R. B. Innis, V. J. Cunningham, J. Delforge, M. Fujita, A. Gjedde, R. N. Gunn, J. Holden, S. Houle, S.-C. Huang, M. Ichise, H. Iida, H. Ito, Y. Kimura, R. A. Koeppe, G. M. Knudsen, J. Knuuti, A. A. Lammertsma, M. Laruelle, J. Logan, R. P. Maguire, M. A. Mintun, E. D. Morris, R. Parsey, J. C. Price, M. Slifstein, V. Sossi, T. Suhara, J. R. Votaw, D. F. Wong, and R. E. Carson, "Consensus nomenclature for in vivo imaging of reversibly binding radioligands," *J. Cerebral Blood Flow Metabol.*, vol. 27, pp. 1533–1539, 2007.

[16] P. M. E. Hawkins, R. A. , and S. C. Huang, "Effects of temporal sampling, glucose metabolic rates, and disruptions of the blood-brain barrier on the FDG model with and without a vascular compartment: Studies in human brain tumors with PET," *J. Cerebral Blood Flow Metabol.*, vol. 6, no. 2, pp. 170–183, Apr. 1986.

[17] R. F. Muzic and S. Cornelius, "COMKAT: Compartment model kinetic analysis tool," *J. Nucl. Med.*, vol. 42, no. 4, pp. 636–645, Apr. 2001.

[18] E. M. Landaw and J. J. DiStefano, "Multiexponential, multicompartmental, and noncompartmental modeling. II. Data analysis and statistical considerations," *Amer. J. Physiol.*, vol. 246, pp. 665–677, 1984.

[19] R. F. Muzic and B. T. Christian, "Evaluation of objective functions for estimation of kinetic parameters," *Med. Phys.*, vol. 33, no. 2, pp. 342–353, 2006.

[20] M. Ishikawa, H. Kikuchi, I. Nagata, S. Yamagata, W. Taki, Y. Yonekura, S. Nishizawa, Y. Iwasaki, and T. Mukai, "Glucose consumption and rate constants for 18F-fluorodeoxyglucose in human gliomas," *Neurologia Medico-chirurgica*, vol. 30, pp. 377–381, 1990.

[21] N. Kimura, Y. Yamamoto, R. Kameyama, T. Hatakeyama, N. Kawai, and Y. Nishiyama, "Diagnostic value of kinetic analysis using dynamic 18F-FDG-PET in patients with malignant primary brain tumor," *Nucl. Med. Commun.*, vol. 30, pp. 602–609, 2009.

[22] A. M. Spence, M. Muzi, D. A. Mankoff, S. F. O'Sullivan, J. M. Link, T. K. Lewellen, B. Lewellen, P. Pham, S. Minoshima, K. Swanson, and K. A. Krohn, "18F-FDG PET of gliomas at delayed intervals: Improved distinction between tumor and normal gray matter," *J. Nucl. Med.*, vol. 45, pp. 1653–1659, 2004.

[23] H. Sari, K. Erlandsson, A. Barnes, D. Atkinson, S. Arridge, S. Ourselin, and B. Hutton, "Exploiting an MRI derived arterial input function to improve the PET simultaneous estimation method: Validation of assumptions," in *Proc. IEEE NSS-MIC Conf. Rec.*, 2014.